Title

The performance of the γ-ray tracking array GRETINA for γ-ray spectroscopy with fast beams of rare isotopes

Authors

Weisshaar, D
Bazin, D
Bender, PC
et al.

Publication Date

2017-03-01

DOI

10.1016/j.nima.2016.12.001

Peer reviewed

The performance of the γ-ray tracking array GRETINA for γ-ray spectroscopy with fast beams of rare isotopes

D. Weisshaar[a], D. Bazin[a,b], P. C. Bender[a], C. M. Campbell[c], F. Recchia[a], V. Bader[a,b], T. Baugher[a,b], J. Belarge[a], M. P. Carpenter[d], H. L. Crawford[c], M. Cromaz[c], B. Elman[a,b], P. Fallon[c], A. Forney[f], A. Gade[a,b], J. Harker[f], N. Kobayashi[a], C. Langer[a], T. Lauritsen[d], I. Y. Lee[c], A. Lemasson[a], B. Longfellow[a,b], E. Lunderberg[a,b], A. O. Macchiavelli[c], K. Miki[a], S. Momiyama[g], S. Noji[a], D. C. Radford[e], M. Scott[a,b], J. Sethi[f], S. R. Stroberg[a,b,1], C. Sullivan[a,b], R. Titus[a,b], A. Wiens[c], S. Williams[a,2], K. Wimmer[a,g], S. Zhu[d]

[a] *National Superconducting Cyclotron Laboratory, Michigan State University, East Lansing, MI 48824*
[b] *Department of Physics and Astronomy, Michigan State University, East Lansing, MI 48824*
[c] *Lawrence Berkeley National Laboratory, Berkeley, CA 94720, USA*
[d] *Argonne National Laboratory, Argonne, IL 60439, USA*
[e] *Oak Ridge National Laboratory, Oak Ridge, TN 37831, USA*
[f] *Department of Chemistry and Biochemistry, University of Maryland. College Park. MD 20742, U.S.A*
[g] *Department of Physics, The University of Tokyo, Hongo, Bunkyo-ku, Tokyo 113-0033, Japan*

Abstract

The γ-ray tracking array GRETINA was coupled to the S800 magnetic spectrometer for spectroscopy with fast beams of rare isotopes at the National Superconducting Cyclotron Laboratory on the campus of Michigan State University. We describe the technical details of this powerful setup and report on GRETINA's performance achieved with source and in-beam measurements. The results reported in this work were obtained from GRETINA consisting of 8 detector modules hosting four high-purity germanium crystals each. Currently, GRETINA consists of 10 detector modules.

Keywords: γ-ray spectroscopy, rare-isotope beams, GRETINA

Email address: weisshaar@nscl.msu.edu (D. Weisshaar)
[1] Present address: TRIUMF, 4004 Wesbrook Mall, Vancouver, British Columbia, V6T 2A3 Canada
[2] Present address: Diamond Light Source, Harwell Science and Innovation Campus, Didcot, Oxfordshire, OX11 0DE, U.K.

1. Introduction

In-beam γ-ray spectroscopy with fast beams of rare isotopes has evolved into a powerful tool for studying the properties of nuclei far away from the valley of β stability. A wide range of experimental techniques has been established to infer experimental information, for example, on collectivity, single-particle structure, and structure information relevant for astrophysical questions [1–3]. The key to those experiments is the use of rare-isotope beams at intermediate energies. These beams of energies up to several hundred MeV/u impinge on a reaction target and the detection and identification of the projectile-like reaction products in coincidence with emitted γ rays quantifies the population of excited final states. The high beam energies allow for the use of reaction targets with thicknesses of several hundred mg/cm^2 for increased luminosity that enables successful γ-ray spectroscopy even at low rare-isotope beam rates of a few particles per second. The same high beam energies, however, also pose a major challenge for the in-beam γ-ray detection as the γ rays emitted by nuclei at velocities exceeding 30% of the speed of light are detected with substantial Doppler shifts in the laboratory reference frame. While this effect can be corrected for up to a certain extent, the achievable energy resolutions of the Doppler-broadened γ-ray lines in the spectra is ultimately limited. This limitation arises from the accuracy of the determination of (i) the emission angle with respect to the trajectory of the γ-ray emitter and (ii) the emitter's velocity at the point of γ-ray decay. The spatial resolution of a γ-ray spectrometer is thus critical and often the constraining factor in the precise determination of the emission angle for the Doppler-shift reconstruction.

Several successful γ-ray spectrometers dedicated to spectroscopy at intermediate beam energies are used at rare-isotope facilities around the world. One class of spectrometers is based on scintillation detectors such as DALI2 (NaI) [4] and CAESAR (CsI(Na)) [5]. The modest intrinsic energy resolution of the detector material allows for a rather coarse granularity before the effect of the Doppler-broadening becomes the dominating factor in the achievable in-beam

energy resolution. Scintillator arrays enable quite compact geometries with 4π coverage around the reaction target, yielding absolute γ-ray efficiencies of 20-30% at 1 MeV. The in-beam energy resolution is typically around 10% full-width-half-maximum (FWHM) at 1 MeV, often limiting the applicability of those devices to experiments with a low number of expected γ-ray transitions well separated in energy.

Spectrometers based on high-purity germanium (Ge) benefit from the vastly improved intrinsic energy resolution as compared to scintillators but need to provide a sufficiently high spatial resolution to retain the superior energy resolution in-beam. This is achieved by employing segmented Ge detectors which enable the identification of the sub volume within the Ge crystal where the γ-ray interactions took place. Examples for such first-generation segmented germanium arrays are GRAPE [6], RISING/MINIBALL [7, 8], and SeGA [9]. For example, SeGA coupled with the S800 spectrograph [10] at the National Superconducting Cyclotron Laboratory (NSCL) at Michigan State University has been a frequently used experimental setup that contributed some of the pioneering in-beam γ-ray spectroscopy measurements to the field of rare isotope science [11].

The **G**amma-**R**ay **E**nergy **T**racking **I**n-beam **N**uclear **A**rray (GRETINA) [12] is one of the first γ-ray spectrometers utilizing the novel concept of γ-ray tracking [13]. In a γ-ray tracking array, the spatial coordinates and deposited energies of each γ-ray interaction are measured. Using the kinematics of the Compton effect, tracking algorithms then reconstruct the scattering paths of the measured γ rays and decide if a γ-ray event was completely absorbed, yielding peak-to-total performances comparable to *Compton-shielded* Ge detector systems. GRETINA, originally consisting of 28 36-fold segmented high-purity germanium detectors mounted in 7 cryostats that house 4 detectors each, provides more than 1π solid-angle coverage. This makes GRETINA especially interesting for spectroscopy with fast beams of rare isotopes, as its compactness allows for good coverage of the solid angle downstream of the reaction target which is advantageous because of the forward focusing of the γ rays in con-

sequence of the Lorentz boost. The spatial resolution provided by GRETINA then enables precise Doppler correction. GRETINA's higher full-energy-peak efficiency, together with its improved peak-to-total performance than that of the first generation segmented Ge detector arrays, permits for the first time high-quality, high-resolution γ-γ coincidence measurements in spectroscopy with fast rare isotopes.

At NSCL, two campaigns of fast-beam experiments with GRETINA coupled to the S800 spectrograph have been carried out [14], with the second campaign still in progress at the time of this work. We describe the setup and technical details relevant for these types of experiments and report on the performance characteristics of GRETINA measured with sources as well as in-beam.

2. The GRETINA-S800 setup

2.1. The GRETINA mechanical support structure

The GRETINA detector support frame consists of two solid Al hemispheres of 12.9 cm thickness and 51.1 cm inner radius. Each hemisphere provides ten mounting holes to support a GRETINA detector module each at a target-detector distance of 18 cm. Two additional mounting positions are shared between both hemispheres at their division line, resulting in 22 detector positions in total. The underlying geometry for a 4π array, like GRETINA's extension GRETA, calls for 30 detector-module positions, namely ten positions in a ring at 90° and five positions each in four rings at 32, 58, 122, and 148° relative to the beam axis. For the GRETINA frame, two mounting positions at 90° are utilized for the axle mechanism supporting the hemispheres and enabling their rotation. Furthermore, in both hemispheres, the section that would nominally support the most forward detector ring at 32° is omitted. The ring at 58° supports only four instead of five detector modules. The 5^{th} position was not implemented in order to provide a recess in the frame which can accommodate the entrance gate valve of the S800 spectrograph. The resulting hemisphere geometry provides the clearances for positioning the center of the GRETINA

array at the pivot point of the S800 spectrograph. The pivot point is located just 37 cm upstream from the entrance gate valve of the S800 and is the preferred location of the reaction target that optimizes ion optics and acceptances of the spectrograph. The support structure of each hemisphere rests on a cart mechanics, allowing the independent movement of each hemisphere.

The two hemispheres are high-precision pieces and were manufactured with tight tolerances. Guided by alignment pins, a GRETINA module slides into alignment during the insertion process into a mounting hole of the hemisphere. Both hemispheres provide fiducial marks for alignment measurements with laser-tracker systems. Over the course of the first GRETINA campaign at NSCL, the positioning of both hemispheres relative to the experimental vault was reconfirmed several times using a laser-tracker system and found to vary by less than 1 mm.

Compared to the sophisticated detector support mechanics, the design of the standard target assembly is simple. The reaction targets used are typically 5 cm $\times$ 5 cm sheets, glued on a plastic (G10) ring of 64 mm inner diameter, 12 mm width, and 0.6 mm thickness. This assembly is then placed on a cradle and pushed down the 6-inch-diameter beam pipe with a push stick of specific length, so that the target on the cradle within the beam pipe is positioned in the center of GRETINA. Also more sophisticated target systems like the TRIPLEX plunger [15] or the liquid hydrogen target [16] have been used. Figure 1 shows a photograph of the area around the reaction target position, with seven GRETINA detector modules mounted in the so-called NSCL standard configuration. In this configuration the four positions at 58^o are populated and all remaining modules are mounted in the 90^o ring. The standard configuration was used for the majority of the experiments carried out with GRETINA at NSCL.

2.2. GRETINA electronics and data acquisition

GRETINA utilizes the modern concept of digital pipelines in its data acquisition architecture. Each digitzer channel triggers and converts events inde-

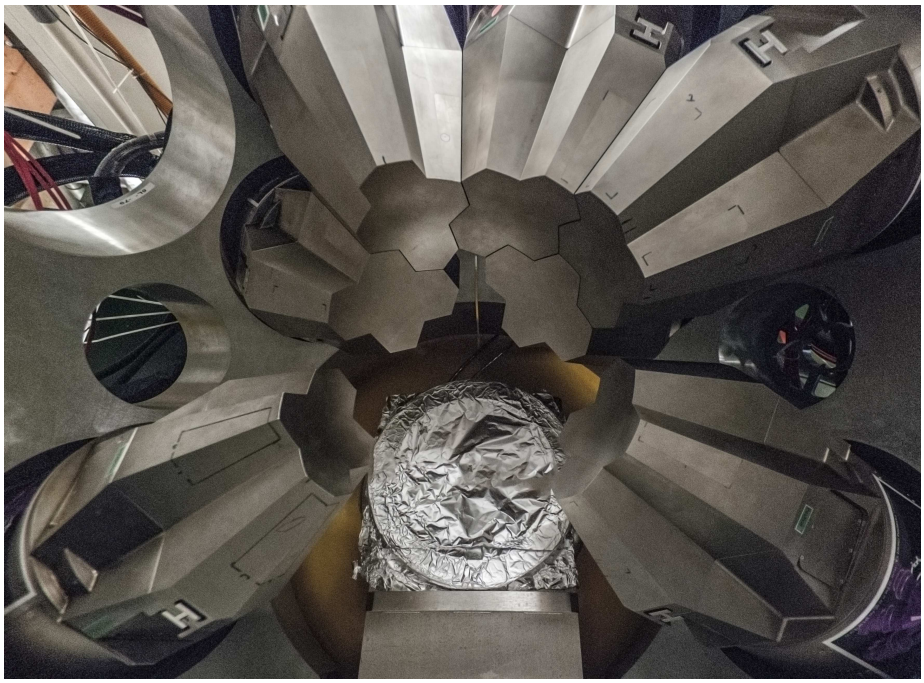

Figure 1: The photograph shows GRETINA in the so-called NSCL standard configuration mounted in front of the S800 spectrograph's entrance gate valve (covered by aluminum foil). Four GRETINA modules are mounted in the 58^o ring and the remaining three modules are located at 90^o. The 6-inch diameter beam pipe is removed for a better view on the detector endcaps. The data discussed in this work were obtained with 8 GRETINA modules, with the 8^{th} module mounted in the free hole seen on the upper left.

pendently, assigns a time stamp, and stores them locally. Those triggers can be derived locally but also provided externally, for example from a Ge detector core contact channel triggering a segment channel. Those triggers are reported to the GRETINA Trigger Timing & Control logic which performs the global trigger decision within the GRETINA system. If a global trigger condition is met, the Trigger Timing & Control logic issues a command to all channels to deliver their locally stored events matching the global trigger by means of time-stamp comparison. This mechanism is called *event validation*. Locally-stored events are dropped if no matching validation is issued within a given expiration time window. The Trigger Timing & Control logic also provides fast trigger signal outputs and accepts external trigger signal inputs from auxiliary detector systems, both crucial ingredients for a coincidence with a particle detection system like the S800 magnetic spectrograph. The latency between a trigger generated locally for a detector channel and the fast trigger signal output is less than 300 ns. Details on the implementation and functionality of the GRETINA electronics and architecture are reported in [17–19].

A Ge-detector crystal raw event is comprised of the digitized signals at 100 MHz sampling rate, energies of the central contact and 36 segment electrodes, and the leading-edge trigger time of the central contact. For that purpose, the conversion of all segment channels is driven by the leading-edge trigger of the corresponding central contact and ensures proper time alignment of the captured signal traces (waveforms). The central contact signal is actually split into four branches and fed into four digitizer channels of 2 MeV, 5 MeV, 10 MeV, and 30 MeV full range, while the segment channels have 10 MeV full range. The length of the captured waveform is typically set to 1.8 μs and results in a raw event length of 16 kB for the 40 digitizer channels instrumenting one Ge crystal.

The global trigger initiates the collection of the raw events from the hit Ge crystals and the data are passed to the GRETINA computer farm that runs the signal-decomposition software. The signal-decomposition process computes the position and energy deposition of the γ-ray interaction points from the measured waveforms [12]. The result, consisting of timing and energy of the

central contact, the energies of the hit segments, and a list of coordinates and energies of each interaction point, is the final Ge-detector event, dubbed *mode2* event. The raw data format, including the captured waveforms that are passed to the signal-decomposition process, is called *mode3* event. While the *mode3* data are usually dropped after the decomposition process, the *mode2* event is passed to the GRETINA event builder process.

The GRETINA event builder receives the Ge-detector events from the many decomposition processes running on the GRETINA computer farm. Each event has a time stamp and a payload of data and the event builder orders them according to the time stamps and writes them to disk. The GRETINA event builder does not build coincidences by combining events with similar or identical time stamp; this task remains for the data analysis. The GRETINA event builder does also accept events from other event sources, such as ancillary detector systems. For online monitoring purposes, the event builder provides an interface for analysis software packages to tap into the built event stream.

The GRETINA computing resources are capable of processing 30,000 γ rays per second. Event buffering allows brief periods exceeding this limit. In case the buffer capacity is exhausted, an inhibit mechanism suppresses further triggers at the front-end electronics until sufficient buffer capacity is restored. The same inhibit mechanism is activated when any component of the GRETINA DAQ system exceeds its data transfer bandwidth. In each data run, the total durations of inhibit periods are measured and reported by the GRETINA DAQ system. For typical experiments performed during the GRETINA campaigns at NSCL, this kind of deadtime is irrelevant as the in-beam trigger rates are well below these limits. It should be noted that, aside from this inhibit mechanism, GRETINA has no global deadtime.

Another source of deadtime in GRETINA is a channel-wise deadtime, related to the local event buffering scheme implemented on the digitizer boards. A local trigger, usually derived from the central contact of the Ge crystal, initiates the conversion and local buffering of the energy filter and waveform data. This processing takes approximately 15-20 μs and acts as a channel deadtime since

the local buffering of any other hit in the same detector occurring during this time window will be discarded. The channel deadtime is monitored and reported for each run as the ratio of locally buffered events and the amount of local triggers. Typical Ge detector rates in in-beam experiments at NSCL were well below 1 kHz which translates into a channel deadtime of 2% or less. For the second campaign of GRETINA at NSCL, the local buffering scheme of the digitizer boards was changed so that only *validated* events are buffered for the readout. Since in the experiments the validation is typically initiated by a particle trigger in the S800 spectrograph, this new buffering scheme is 100% efficient as long as a second event does not occur in the same digitizer channel during the validation window of typical $4 - 6$ μs length. However, events that close in time would pile-up in energy in any case.

2.3. The data acquisition system of the S800 spectrograph

The data acquisition architecture used for the magnetic S800 spectrograph is based on a classic event-by-event readout scheme. The event readout is initiated by a master trigger signal, prompting the conversion for all detector channels, for example amplitude conversion in ADC modules or timing in TDC modules. After conversion, the data are read out from the modules by the corresponding crate controllers and transferred to an acquisition computer via a USB interface. Depending on the number of detector channels fired, the whole readout process takes 120-200 μs. No other master trigger can be issued during this period.

The generation of the master trigger is controlled by the versatile trigger logic of the S800 spectrograph. The logic allows trigger conditions to be set on multiple trigger sources as well as coincidence conditions between two trigger sources. The fast focal-plane scintillator is usually taken as the trigger source for the S800 spectrograph. A time stamp mechanism assigns a time stamp for each event. It is implemented as a counter which runs on clock cycles provided by an internal or external clock source at a frequency of up to 20 MHz. For deadtime determination, the S800 DAQ system offers scaler data, counting the input count rate of the several trigger sources and the number of generated

triggers. A 10 kHz clock signal and a copy of it vetoed by the S800 DAQ busy signal are recorded by the scaler modules as well and provide a direct measure of the livetime of the system.

2.4. Interfacing GRETINA and S800

Combining the S800 spectrograph and GRETINA is accomplished through the time stamps that both data acquisition systems provide. Time-stamp synchronization between both systems is achieved by providing the GRETINA clock signal, downscaled to 12.5 MHz, as a reference for the S800 time-stamp counter. At the start of a data taking run, all time-stamp counters are reset to zero, allowing coincidence correlation of S800-GRETINA events by means of a simple time-stamp comparison. While the S800 focal plane detectors can tolerate count rates of up to 6-10 kHz, deadtime considerations make it desirable to limit the master-trigger rate to 1.5 kHz or less. For that purpose, the fast trigger output from the GRETINA Trigger Timing & Control logic is used in the S800 trigger logic to form the GRETINA-S800 coincidences, reducing the master trigger rate in the S800 DAQ system. A coincidence window width of 600 ns is typically used to accommodate the time walk in the GRETINA trigger signals originating from the leading-edge discriminator algorithms used on the GRETINA digitizer boards. The master trigger from the S800 logic is also sent to the GRETINA Trigger Timing & Control logic and used to validate events in GRETINA with a validation window width of typically 4 μs or longer.

The granularity of the 12.5 MHz time-stamp clock is sufficient for the correlation of S800-GRETINA coincidences, but not to recover the detector timing properties between the Ge detectors of GRETINA and the scintillators of the S800 spectrograph. Therefore, the master trigger signal from the S800 DAQ is also fed into a dedicated digitizer card in GRETINA and read out by the GRETINA DAQ. This provides an S800 timing reference in GRETINA since all timing measurements in the S800 system are performed relative to the master trigger. The quality of this timing reference is sufficient to recover the Ge detector timing performance of 10 ns relative to a fast plastic scintillator signal

from the S800. Master trigger signals are at least 100 μs apart in time because of the duration of an S800 readout cycle. This separation is significantly longer than the digitizer channel deadtime and ensures that the master trigger signals are processed in the dedicated digitizer in GRETINA with essentially 100% efficiency. This property is routinely used as a diagnostic tool, namely every S800 event has to have its counterpart in the GRETINA event stream.

The event data measured by the S800 DAQ are sent to the GRETINA event builder process where they are merged with the GRETINA data and stored. The combined data stream is also made available for online data analysis and monitoring of the proper operation of all detector channels.

3. Source measurements

3.1. Energy resolution and γ-γ timing

During its operation at NSCL, GRETINA was thoroughly characterized with γ-ray calibration sources. Energy resolutions of 1.6 keV at 122 keV and 2.4 keV at 1332 keV were extracted from the spectrum sum of all 32 individual crystal singles spectra in the second campaign. For the first campaign, worse resolutions of 2.2 keV at 122 keV and 2.8 keV at 1332 keV were measured and traced back to a less sophisticated energy algorithm implemented on the digitizer firmware at the time.

The detector timing characteristic was measured from γ-γ coincidences with a ^{60}Co source. For each detector, the decomposition process reports the time stamp of the leading-edge trigger and the so-called t_0 value. The time t_0 describes the signal start in a trace ensemble of a crystal and is a fit parameter computed in the signal decomposition process. As the traces are aligned and read out relative to the leading-edge trigger, the sum of the leading-edge time value and t_0 provides the detector time with sub-bin timing granularity. The γ-γ coincidence timing for events with two or more detectors fired is calculated as the difference between those detector times, while the time of the detector reporting the highest energy is taken as the timing reference. A coincidence

timing resolution of 14 ns FWHM was achieved for all GRETINA events gated on the 1173 keV-1332 keV coincidences. This value worsens to 20 ns when the 1173 keV gate is changed to detected γ-ray energies of around 300 keV (Compton events) in the same data. At this energy of 300 keV, the timing peak starts to develop an additional structure towards later detector times, extending up to 300 ns. At 300 keV this region of events with worse timing contains around 5% of the events while at 100 keV this number increases to 40%. As a consequence, careful consideration is needed for placing time gates in the analysis of low-energy γ-ray yields, as too tightly set timing gates can easily cut into GRETINA's low-energy efficiency.

3.2. Absolute efficiency

In many experiments with GRETINA at NSCL, a primary experimental observable is the cross section for populating excited states, tagged by their prompt γ decays as measured in GRETINA. Therefore, the absolute detection efficiency of the S800-GRETINA setup is a crucial performance parameter and was thoroughly characterized for each of the detector configuration realized at NSCL. One efficiency commonly quoted for tracking arrays is the calorimeter efficiency for sources with γ-ray multiplicity 1, for which all energies detected in an event are added first and put in a single spectrum. Obviously, for ^{60}Co and any other calibration source with γ-ray multiplicity larger than 1, the calorimeter spectrum will likely collect contributions from all coincident γ rays in an event, making the extraction of a calorimeter efficiency from those spectra a challenging task [20]. The calorimeter efficiency describes the upper limit for the efficiency achievable after the tracking procedure and is therefore an important benchmark for a tracking array. The calorimeter efficiency depends on the detector arrangement as it is more likely to recover γ rays scattering out of one crystal into another the more compact the configuration is. Of course, for in-beam experiments with γ multiplicities that are typically larger than 1, the calorimeter efficiency has less relevance.

The singles efficiency of a tracking array can be measured more easily. For

that, the individual spectra of each Ge crystal are summed into one singles spectrum that is then analyzed. For calibration sources with low γ-ray multiplicity any contribution from cross scattering removing a good full-energy-peak count from the peak in the spectrum, as well as the probability that more than one γ ray is emitted towards the same detector crystal in an event are considered to be negligible. The latter assumption is justified as a Ge crystal is covering less than 1% of the 4π solid angle. Another advantage of extracting a singles efficiency is that this efficiency stays the same for different array configurations.

3.2.1. The GRETINA singles efficiency

The measured singles efficiency curve for GRETINA consisting of 32 crystals is shown in figure 2. The calibration sources used had activities of less than 2 μCi and produced a rate of several hundred Hz per Ge crystal, causing a total trigger rate of up to 25 kHz in GRETINA. The GRETINA computer farm can handle this rate of signal decomposition processes and so all source calibration data were taken in the same acquisition mode of GRETINA as the in-beam data. The absolute efficiency of the array was extracted using a ^{152}Eu source with known activity, the peak integrals in the acquired spectra, the γ-ray yield per disintegration [21], and the acquisition time corrected for the deadtime. This deadtime correction is small (< 2 %) in the case that the GRETINA readout was triggered locally by the GRETINA Trigger Timing & Control logic since only the channel deadtime of 15 μs has to be considered. In the case that the GRETINA fast trigger signal was used in the S800 trigger logic to trigger a γ-ray event, the deadtime was considerable at about 60-70%, as each trigger also initiated a readout cycle in the S800 DAQ as well. This deadtime was obtained solely from the S800 deadtime measurement using its raw and live clock measurements. In either trigger mode, the same absolute singles efficiency for the ^{152}Eu source was extracted, proving the validity of the deadtime measurement. The error bars for the ^{152}Eu data points are given by the uncertainty of the γ-ray yields and the source activity. The activity of the ^{152}Eu calibration source is quoted with 1.4% accuracy by the manufacturer.

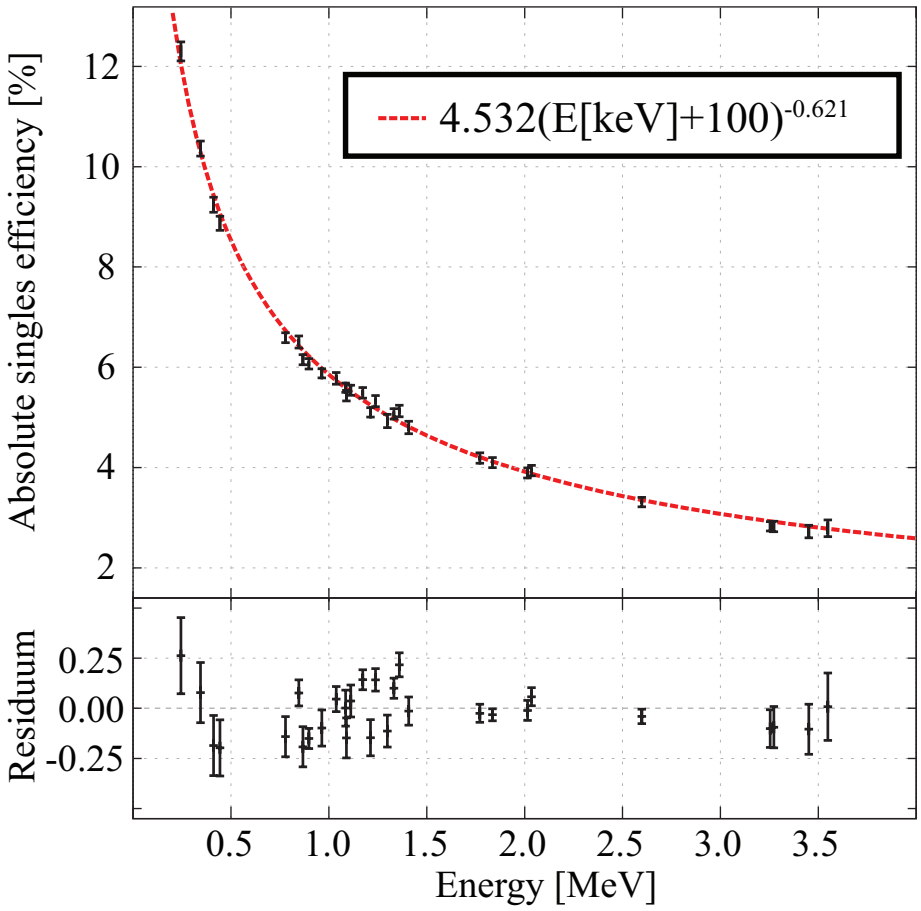

Figure 2: The singles efficiency of GRETINA consisting of 8 detector modules is shown. The curve following the data points is parametrized as $4.532 \cdot (\mathrm{E[keV]}+100)^{-0.621}$. The weighted standard deviation between data points and curve is 2.1%.

Absolute efficiency data points were also determined with ^{60}Co and ^{88}Y using coincidences with a $LaBr_3$:Ce scintillation detector. The strategy of this measurement with a multiplicity 2 source is that for any full-energy-peak event measured in the scintillator, the coincident γ ray must have been present and may or may not be detected in GRETINA. Absolute efficiencies can then be extracted from the ratio of the full-energy-peak events detected in GRETINA in coincidence with the corresponding energy in the $LaBr_3$:Ce scintillator divided by the number of full-energy-peak events recorded in the scintillator in singles. Practically, the signal of the $LaBr_3$:Ce scintillator was fed into the S800 spectrograph electronics, replacing the signal of the focal plane trigger detector. The trigger condition of the S800-GRETINA DAQ was set on S800 singles, i.e. in this case $LaBr_3$:Ce singles. Offline, the GRETINA singles spectrum for events in coincidences with the corresponding full-energy-peak events in the $LaBr_3$:Ce scintillator was created. If the software energy gate is set on the higher-lying ^{60}Co line in the $LaBr_3$:Ce detector spectrum, then the absolute efficiency is the ratio of the full-energy-peak counts obtained from the GRETINA singles spectrum over the number of events in the scintillator that satisfy the same energy gate condition [3]. Still, two corrections must be considered. The first correction is the random coincidence rate which can be estimated from the amount of full-energy-peak events of the higher line seen in the gated GRETINA spectrum, i.e. the 1.33 MeV line still seen in GRETINA while gated on 1.33 MeV in the $LaBr_3$:Ce detector. For the low-activity sources used, this effect is in the order of 10^{-3}, so for every 1000 counts observed in the 1.17 MeV peak in the gated GRETINA spectrum just 1-2 counts appear in the 1.33 MeV peak due to random coincidences. A second correction is needed to account for the γ-γ angular correlation [22] and can be calculated from the correlation coefficients [21] and the array configuration. For the data presented here, this correction was computed to be of the order of 1-3 % for the different configurations and is

[3] For ^{88}Y the β-decay branch directly feeding the 1836 keV level needs to be considered, too.

included in the quoted efficiency. When the energy gate condition is set on the lower-lying line in the $LaBr_3$:Ce scintillator singles spectrum, one needs to consider that the higher γ energy, scattered out of the scintillator, may also satisfy the same energy gate condition. This can be seen in the coincident GRETINA singles spectrum, which shows a considerable peak for the lower energy in addition to the higher energy line. From its peak integral, the number of those events scattering out of the scintillator can be estimated. In the data presented here, 2-4% of the $LaBr_3$:Ce singles events in the gate for the lower energy line stem from those scatters. Using the method outlined in this paragraph, the absolute singles efficiency of GRETINA (consisting of 8 detector modules) at 898 keV, 1173 keV, 1332 keV, and 1836 keV are 6.08(4)%, 5.49(5)%, 5.07(5)%, and 4.06(3)%. The errors quoted are statistical.

A singles measurement with a ^{56}Co source was used for accessing the efficiency beyond 1.84 MeV. The activity of that source was unknown and so the relative efficiency was extracted and scaled to best fit with the absolute efficiency points in the energy region from 800 keV to 2 MeV. These scaled ^{56}Co data points and the absolute efficiency data points obtained with the ^{152}Eu source and the $LaBr_3$:Ce coincidence measurements are shown in figure 2 and used to extract the overall experimental efficiency curve shown in the same figure. The error of the efficiency curve can be estimated from the residuum distribution centered at 0 with a σ of 0.11. Most data points that contribute to the residuum are located in the energy region from 1 to 1.5 MeV with an absolute efficiency value of $\epsilon_{singles} \approx 5\%$, so one may conclude that the efficiency curve overall describes the efficiency within 2-3% accuracy.

3.3. Calorimeter and nearest-neighbor add-back mode

The singles efficiency does not capitalize on the capability of GRETINA to recover the energy of γ rays scattered between crystals. It is ultimately the task of a tracking algorithm to combine the measured interaction points to a full-energy-peak γ-ray event. The gain in counts in a peak for a particular tracking strategy can be measured relative to the peak counts obtained in the

singles spectrum and is called the add-back factor. The add-back factors for the calorimeter mode at γ-ray multiplicity 1 and energies of 898 keV, 1173 keV, 1332 keV, and 1836 keV were extracted from the $LaBr_3$:Ce coincidence data as 1.416(5), 1.453(5), 1.470(5), and 1.544(5). Those values were obtained for GRETINA in NSCL's standard configuration consisting of 8 detector modules and an energy threshold of ≈ 50 keV. At 1.3 MeV, this translates into a calorimeter efficiency of 7.3% using the singles efficiency value from the efficiency curve parametrization from figure 2.

Though the add-back analysis appears to be a relative measurement, it is necessary to consider the impact of deadtime and random coincidences. The latter may remove counts from the full-energy peak in the calorimeter spectrum in case of a random coincidence. For γ-ray multiplicity=1, this effect can be conveniently estimated by comparing the full-energy-peak counts in the singles spectrum with the calorimeter spectrum, where the latter spectrum is gated on detector fold=1 events. Because a full-energy-peak count in the singles spectrum implies that exactly one crystal was hit, the same number of counts is expected in the corresponding, fold-one-gated calorimeter spectrum if no random coincidence increased the measured detector fold. The ratio of peak counts in the fold-one calorimeter spectrum over peak counts in the singles spectrum provides a measure of the impact of random coincidences. Because only weak sources were used for the data presented here, the value of this measure turned out to be insignificant (>0.995), and therefore no corrections attributed to random coincidences were needed or applied. It is worthwhile to note that a similar analysis can be performed for γ-ray multiplicities>1 if the sum peak is investigated instead of the peaks from the individual γ-ray transitions. Concerning the deadtime, the channel deadtime in GRETINA leads to a detector-fold dependent deadtime. If $LT_{chn} = (1 - DT_{chn})$ describes the channel livetime (LT) and deadtime (DT), then the probability for *all* hit detectors in an n-fold event to be alive is given as $(LT_{chn})^n$. Naturally, if one or more hit detectors are not alive in a full-energy-peak event, the energies of the remaining detectors cannot add up to the full-energy-peak in the spectrum and this event is then wrongly accounted

as Compton background. For the data discussed here, this effect is small and deemed negligible since the low count rates translate into $LT_{chn} > 0.99$ and the detector fold is usually 1-2. For example, for the 1.84 MeV full-energy-peak events from ^{88}Y only 5% of the events have a detector fold larger than 2.

As mentioned earlier in this section, the calorimeter mode is not a viable mode for in-beam spectroscopy as one usually encounters γ-ray multiplicities exceeding 1. A simple approach to recover the cross-scattered γ rays to some extent is the so-called nearest-neighbor add-back procedure. Two detectors are called nearest neighbors when they share a common boundary, such as two crystals next to one another within a cryostat as well as two crystals next to one another in two adjacent GRETINA modules. Four different spectrum types are defined:

- *n0-spectrum*: This spectrum is incremented for each hit detector when none of its nearest neighbor detectors has fired.

- *n1-spectrum*: Two detectors A, B which are nearest neighbors have fired, and all other nearest neighbor detectors of A and B have not fired. In this case, the energies from detector A and B are added and the result is incremented in the n1-spectrum.

- *n2-spectrum*: Three detectors A, B, and C are all pair-wise nearest neighbors and have fired and all other nearest neighbors of A, B, or C have not registered a hit. All three energies are added and the sum is incremented in the n2-spectrum.

- *ng-spectrum*: Collects all detector events which do not fulfill the n0, n1, or n2 conditions. No adding of energies is done.

The idea behind this simple approach is that if nearest-neighbor detectors have fired, it is more likely that a γ ray scattered from one detector into another than that two coincident γ rays were detected. If several neighboring detectors have fired, like three detectors A, B, and C in a row, meaning A and C are both nearest neighbors of B, but A and C are not nearest neighbors, the situation

becomes unclear and those events are collected in the ng-spectrum as three counts at the energies seen in detectors A, B, and C. The spectra n0, n1, and sometimes n2 are added into one add-back spectrum and the add-back factor can be extracted from the gain in peak counts with respect to the singles spectrum. In figure 3, the singles and add-back spectra obtained from a ^{60}Co source run taken in the 8 GRETINA module standard configuration are shown. Here, only n0 and n1 spectra were added together. For the 1.33 MeV line, one can see the more than 30% gain in statistics. One also notes the six-fold gain in statistics for the sum peak of the 1.17 MeV and 1.33 MeV at 2506 keV. For the sum spectrum, naively one may expect just a gain of two as only two detectors are added, i.e. covering twice the solid angle. But the logic for the n1 spectrum implies that *any* neighbor can be hit, and as a crystal has on average four neighbors in this particular array configuration, the increase in solid angle coverage is five-fold, close to the observed add-back gain of six for the sum peak. If the add-back spectrum is made from n0, n1, and n2, the add-back gain for the sum peak increases from 6.16 to 10.15, while for the 1.33 MeV line only an increase from 1.33 to 1.36 is seen. Close to the sum peak energy, the 2614 keV line is again a single γ ray from natural background radiation, and its much smaller add-back factor underlines that the much larger gain for 2506 keV peak is solely due to the sum-peak characteristics. The same figure shows in the bottom panel the ng spectrum for the same energies. Its small full-energy-peak statistics compared to the add-back statistics ($< 10^{-3}$) justifies discarding those events when creating an add-back spectrum.

Table 1 summarizes the add-back factors measured for different γ-ray energies for 8 GRETINA modules in the NSCL standard configuration. Add-back factors are given at individual γ-ray energies for n0-n1 and n0-n1-n2 add-back spectra as well as for the calorimeter mode when the coincidence method with the $LaBr_3$:Ce scintillator was used. For the ^{60}Co and ^{88}Y source measurements without an ancillary trigger detector, the add-back factors at the higher γ energy are given only for n0-n1 and n0-n1-n2 spectra, since the calorimeter spectrum is dominated by the summing effect of the two coincident γ rays. The add-back

factors seen here are smaller for the same reason, namely that both γ rays can interact in the same solid angle in GRETINA, therefore producing a crystal hit pattern not meeting the n0, n1, or n2 condition, or summing up to the wrong energy. Comparing the calorimeter add-back factors with the n0-n1 add-back shows that these values differ by less than 10%, or in other words, the simple n0-n1 add-back already recovers more than 90% of GRETINA's calorimeter full-energy-peak efficiency. Contrary to the calorimeter mode, the nearest-neighbor add-back routine can be applied in measurements with modest γ-ray multiplicities as the ones that have been part of NSCL's fast-beam campaigns. When the n0-n1-n2 add-back is performed, the add-back factor increases only marginally by 2-3% as compared to the n0-n1 add-back, but as discussed in the previous paragraph, at the expense that any sum peak would gain 50% or more in statistics.

The same table 1 also lists the peak-to-total values obtained from the spectra. The peak intensities of the corresponding γ-ray transitions were obtained from a simple integral over the peak region corrected for the background estimated from a linear interpolation between the regions left and right from the peak. The total counts were obtained as the spectrum integral from 150 keV up to (and including) the peak of the highest γ-ray transition observed from the source. The sum-peak and the region beyond the peak of the most energetic transition were *not* considered in the peak-to-total evaluation. The values show that the peak-to-total values for the calorimeter mode and the add-back modes are not far apart, and both are a significant improvement as compared to results for the singles spectra. For the peak-to-total results of the source measurement without ancillary coincidences, the values are essentially the mean value from the two corresponding γ-ray lines, showing that the γ-ray multiplicity of 2 does not significantly impact the n0-n1 and n0-n1-n2 add-back. Furthermore, both add-back approaches deliver nearly identical performances in terms of peak-to-total.

In summary, the simple add-back algorithm described here is an efficient procedure which recovers more than 90% of the spectral performance of the

GRETINA calorimeter properties in terms of efficiency and peak-to-total. In contrast to the calorimeter mode, which is only a viable option for a γ-ray multiplicity of 1, the nearest-neighbor add-back approach can be applied to data of moderate γ-ray multiplicity.

	Add-back factor			peak-to-total			
	calorimeter	n0n1	n0n1n2	singles	calorimeter	n0n1	n0n1n2
1.86 MeV	1.53	1.42	1.46	0.171	0.324	0.294	0.296
1.33 MeV	1.46	1.36	1.40	0.208	0.355	0.337	0.339
1.17 MeV	1.45	1.36	1.39	0.225	0.394	0.362	0.365
898 keV	1.41	1.33	1.35	0.254	0.428	0.397	0.398
^{60}Co	n.a.	1.33	1.36	0.229	n.a.	0.360	0.362
^{88}Y	n.a.	1.37	1.41	0.216	n.a.	0.348	0.349

Table 1: Summary of the measured add-back factors and peak-to-total values obtained with ^{60}Co and ^{88}Y sources for the calorimeter mode and the add-back procedure. For the individual energies listed in the upper four rows, the single-peak spectrum was analyzed which was extracted in coincidence with a LaBr detector. For the two bottom rows the source spectra were measured in GRETINA without an additional LaBr detector and the add-back factor is given for the higher energy. For those spectra, as the γ-ray multiplicity is >1, the determination of an add-back factor or peak-to-total is not applicable for the calorimeter mode (see text).

4. Performance of GRETINA for in-beam spectroscopy at intermediate beam energies

Experiments utilizing fast beams of rare isotopes at NSCL are typically carried out at beam energies of 80-100 MeV/u. This corresponds to velocities of 40% the speed of light and leads to considerable Doppler-shift and Lorentz-boost effects of the γ rays measured in the laboratory frame. Both effects needs to be

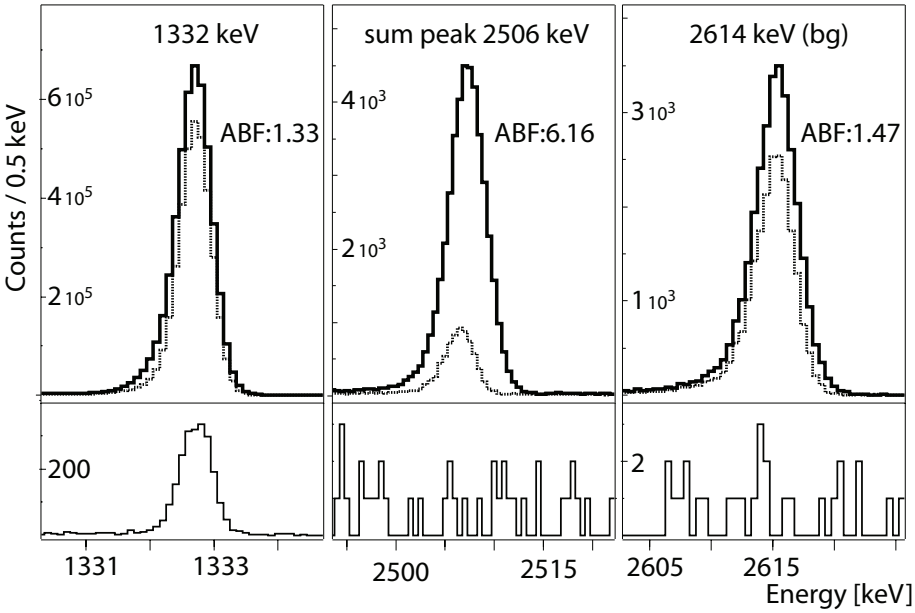

Figure 3: The figure compares the peaks at 1.33 MeV, 2.51 MeV (sum peak), and 2.61 MeV (background) obtained as singles and with add-back (*n0* and *n1*) in the top row. The bottom row shows the counts that were identified as *ng*, a measure of the counts discarded in the proposed add-back procedure.

accounted and corrected for to achieve optimal energy resolution in the measured γ-ray spectra and valid γ-ray efficiencies. The impact of angular distribution on the in-beam efficiency may need to be considered as well, depending on the alignment of the γ-ray emitting reaction products, see for example [23]. For the data presented in this work the angular distributions measured in the laboratory system were compatible with an isotropic distribution in the rest frame of the γ-ray emitting fragments.

4.1. Doppler-shift reconstruction

The relationship between a γ-ray energy, E_{rest}, emitted in the rest frame of a nucleus moving at a velocity v in the laboratory system and the γ-ray energy, E_{lab}, observed is given as

$$E_{rest} = E_{lab}\frac{1-\beta\ \cos(\theta)}{\sqrt{1-\beta^2}} \tag{1}$$

with $\beta = v/c$, c the speed of light, and θ is the observation angle in the laboratory with respect to the direction of $\vec{v}$.

For studying the Doppler-shift correction capability of GRETINA, excited states in ^{28}Si were populated in a multi-nucleon removal reaction from a ^{36}Ar beam at 86 MeV/u on a 100 mg/cm^2 Be target located at the center of GRETINA. The reaction residues were detected and identified event-by-event in the focal plane of the S800 spectrograph. Though the selected spectrograph setting was centered on ^{34}Ar, the two-neutron removal channel, the projectile fragmentation leading to ^{28}Si was one of the strongest reaction channels observed in the focal plane and provided a high-statistics data set of Doppler-shifted 1779 keV γ rays from its $2^+ \rightarrow 0^+$ transition. In this measurement, GRETINA was set up with four modules at 58° and four modules at 90°.

In the simplest application of eq. 1 the angle θ is reconstructed event-by-event relative to the beam axis using the coordinates of the first interaction of the γ ray in GRETINA and the location of the target. As the first interaction,

the coordinates of the hit with the highest-energy deposition is chosen, the so called *main* interaction. For β, a fixed mean value is used which lines up the reconstructed peak at the proper energy of 1779 keV for every GRETINA detector. In this specific case β=0.3722 was used. With this correction, an energy resolution of 2.8% (FWHM) of the 1779 keV line is achieved in the Doppler-reconstructed γ-ray singles spectrum. The measured energy resolution improves to 1.1% if the angle θ in eq. 1 is instead calculated event-by-event with respect to the particle trajectory at the target location as ray traced from focal-plane data of the S800 spectrograph. This significant improvement is expected as the scattering angles of ^{28}Si residues cover the full angular acceptance of the S800 (about $\pm$60 mrad), while the accuracy of the trajectory reconstructed with the spectrograph is on the order of a few mrad and the position resolution of 4-5 mm FWHM in GRETINA translates into an angle resolution of $\approx$20 mrad (FWHM).

The energy resolution after Doppler reconstruction is improved further to 1.0% by taking into account an event-by-event correction for the value of β used in eq. 1. Besides the reconstructed dispersive and non-dispersive scattering angles used for calculating the particle's trajectory, the S800 spectrograph also provides a value for dT/T where T is the kinetic energy of the fragment. Using the relativistic relationship

$$\frac{d\beta}{\beta} = \frac{1}{\gamma(\gamma+1)}\frac{dT}{T} \tag{2}$$

with $\gamma = 1/(\sqrt{1-\beta^2})$ allows an event-by-event correction, $d\beta$, to the fixed value of β. It should be noted that dT/T is the kinetic energy measurement of the fragment *behind* the target, and thus not necessarily at the time the γ-ray emission occurred. In experiments at the lowest reaction rates, usually thicker targets are used for GRETINA-S800 science experiments to increase the luminosity, causing significant energy-loss (velocity change) in the target, rendering this correction without effect for those cases.

The non-dispersive position of the reaction residue at the target is also reconstructed event-by-event. The angle θ in eq. 1 can be refined by using this value to adjust the location of the γ-ray emission. In the data discussed here, this particular correction had no impact as the incoming (stable) ^{36}Ar beam profile had a small spread in the non-dispersive direction. However, the GRETINA campaign did include experiments for which this correction yielded a measurable improvement of the energy resolution.

The statistics collected for the 1779 keV line were sufficient to investigate this peak in each individual detector crystal. Shown in figure 4 are the peak centroids, correlated with the azimuthal position of the corresponding crystals. So far in the Doppler-shift reconstruction, the incoming beam is assumed to coincide with the optical beam axis, thereby placing the location of the γ-ray emission at the center of GRETINA. For the forward detectors a clear correlation can be seen that is less pronounced for the detectors at 90°. This suggests that the point of the γ-ray emission has an offset relative to the optical beam axis, changing the observation angle θ in eq.1 for the forward detectors but with minor impact for detectors located closer to 90°. In cases where the beam hits the target with an offset angle with respect to the beam axis, the same correlation would be seen for all detectors, independent of their polar position. This observation justifies the last step in the Doppler-reconstruction procedure, namely varying a five-parameter set describing a beam spot offset (x, y), target offset z, and beam angle offset (θ_{beam}, ϕ_{beam}) which aligns the centroids measured in the individual crystals. For the data discussed here, the optimized parameter set moves the beam spot by 5 mm perpendicular with respect to the optical beam axis and sets the beam offset angle θ_{beam} at 2 mrad. With those offset parameters applied for the Doppler-shift reconstruction, the measured centroids scatter around the mean value of 1779 keV with a standard deviation of less than 1 keV. The maximum discrepancy is 2.2 keV, found for a crystal at a polar angle of 75°. Assuming that this energy shift is entirely caused by an improper angle used in the Doppler-shift procedure, this energy shift translates into an angle shift of 3 mrad. At a distance of 200 mm, this angle corresponds to

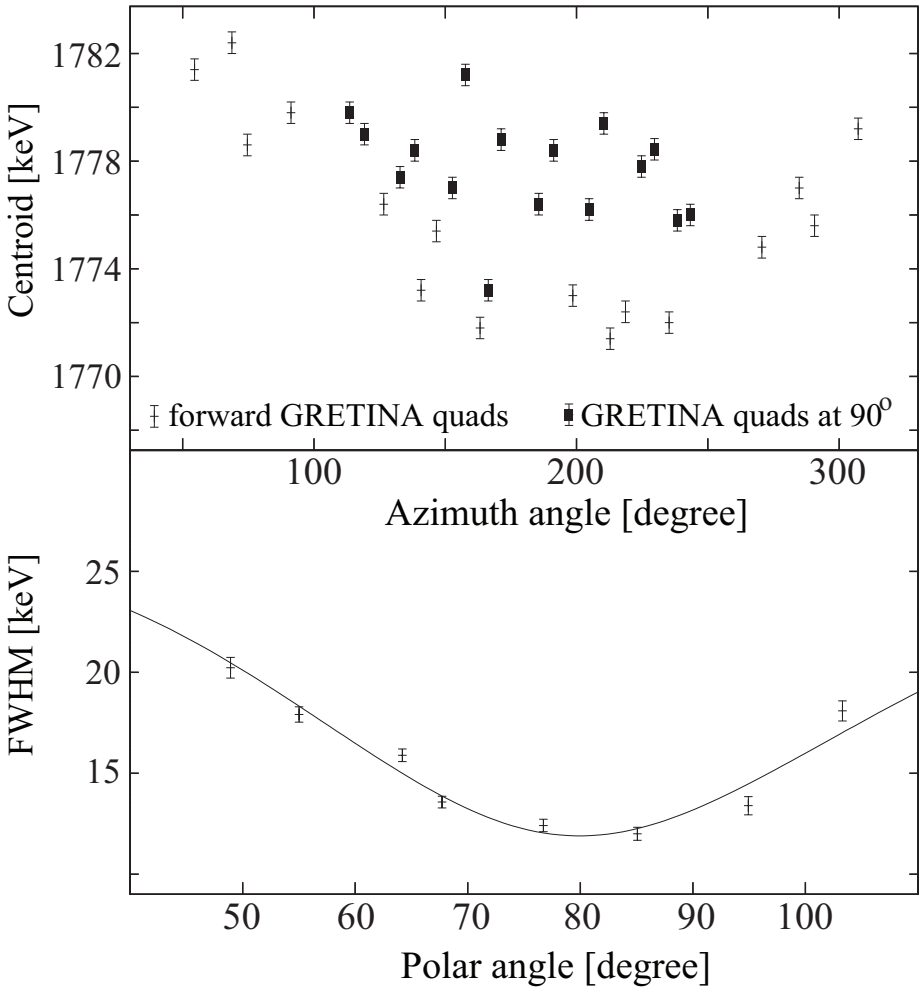

Figure 4: The top graph shows the centroids of the $2^+ \rightarrow 0^+$ transitions in ^{28}Si measured in the individual GRETINA crystals after Doppler-shift correction assuming that the mean ^{28}Si trajectory runs along the optical beam axis. The abscissa describes the azimuth angle of the individual crystals. The bottom graph shows the full-width-half-maximum obtained with the crystals at the different polar angles. The curve shows a fit of a function describing the Doppler broadening.

a displacement of just 0.6 mm. This is a remarkable precision considering that the interaction points used are measured in the crystal coordinate system and then translated into the lab system, using the nominal detector positions given by the computer model of GRETINA. This result underlines the precision of the frame mechanics and the tight tolerances of the detector assemblies themselves as delivered by the manufacturer.

In terms of resolution, the 1779 keV transition is measured with a FWHM of 0.9% when all corrections discussed above are applied. Figure 4 gives the energy resolution after Doppler-shift reconstruction averaged for detector crystals at similar polar angles, plotted versus the observation angle. The curve in the same plot is the result of fitting the formula for Doppler broadening as reported in eq. 5 of Ref. [2]. The uncertainty $\Delta\beta = 0.012$ is in good agreement with the expectation from an energy-loss calculation. The uncertainty $\Delta\theta$ has a contribution of 14 mrad for the detection angle. Also, the beam spot size in the dispersive direction needs to be taken into account. It is modeled as 36 mrad $\times \cos(\theta)$ and is considered as an additional contribution to $\Delta\theta$. The value of 36 mrad corresponds to a spot size of 7 mm, and is in agreement with the beam profile imaged during the beam tuning on a viewer target placed at the target position. Note, that the fit values are given as FWHM, not σ. The value of 14 mrad for the detection angle resolution translates at a 200 mm distance into a position resolution of σ=1.2 mm and is significantly better than the position resolution of 1.9 mm reported in [12]. An explanation may relate to the γ-ray energy. In [12] the position resolution was obtained with a ^{137}Cs source at 662 keV, while in this work, a three times higher γ-ray energy is investigated.

The γ-ray peak resulting in a FWHM of 0.9% is shown in panel a) of figure 5. The shape of the peak is not Gaussian but shows extended tails to both sides. Panel c) shows the same data, but the center-of-mass coordinates of the segment with the highest energy deposition are used for the Doppler-shift correction. The significant improvement from c) to a) is obvious.

4.2. Using tracking for first-hit identification

A simple tracking algorithm was evaluated for the identification of the first hit. If several interaction points in a crystal are reported by the decomposition process, this algorithm calculates for all possible sequences a figure-of-merit (FoM) defined as

$$FoM = \sum \frac{(\cos\Theta^i_{en} - \cos\Theta^i_{vec})^2}{w_i} \tag{3}$$

with Θ^i_{vec} the geometric angle that uses the coordinates of the interaction points and Θ^i_{en} the angle obtained from the energy depositions at those interaction points using the Compton scattering formula. The sum runs over all scatters in the sequence of points with the center of GRETINA fixed as the origin of the γ-ray emission and the initial γ-ray energy taken as the total energy measured in the crystal. The parameter w_i is a weight and usually chosen as the number of interactions. The advantage of using the cosine of the angles is the simple treatment of cases where the reported energies result in a solution with $\cos\ \Theta^i_{en} < -1$ for the Compton formula, which are naturally taken care of in this definition for the FoM.

Of all possible permutations, the sequence with the smallest FoM value, FoM^{min}_{trk}, is considered the most compatible with the Compton-scattering process and the coordinate of the first interaction point in this scattering sequence is taken for the Doppler-shift correction. In order to compare with the main-interaction approach, a further value FoM^{min}_{main} is obtained in the same fashion, but with the main interaction point fixed as the first interaction for all permutations. Therefore, the value of FoM^{min}_{main} is always greater than or equal to FoM^{min}_{trk}. They are equal if the main interaction point and tracked first interaction point coincide.

Applied to the 1779 keV transition from the data on ^{28}Si as shown in figure 5, this approach reports that the main interaction and tracked first interaction are identical for about half of the peak counts. For events where those interactions are different, panel b) in figure 5 shows the Doppler-reconstructed spectrum using the main interaction coordinates, while in panel d), for the same events,

the tracked first interaction coordinates are used. The superior resolution of the peak using the main interaction is obvious and shows experimentally that the main interaction is a valid approximation for the coordinates of the first interaction in a position sensitive detector.

Comparing spectrum b) with a) in figure 5 shows that the peak base appears to be broader in b). A comparison was done with the Doppler-reconstructed spectrum only containing the events for which the reported tracked first interaction and main interaction are identical, which is equivalent to the spectrum difference between a) and b). This spectrum shows a FWHM improved by 15% compared to b) and the width at one tenth of the maximum shows an improvement of 30%, indicating a substantial reduction of the tails extending to both sides of the peak.

A subset of the data was identified where the use of the first tracked interaction for the Doppler reconstruction led to an improvement of about 30% FWHM as compared to using the main interaction. This subset consists of events where the number of interactions reported by the decomposition process equals the number of hit segments in the crystal, and the differences between FoM^{min}_{main} and FoM^{min}_{trk} are in the range of 1 to 3. If instead for the FoM difference a range of 0.1 to 1, or greater than 3 is chosen, correcting with respect to the main interaction results in narrower peak shapes. A weight $w_i = 1$ was used for computing those FoM values according to eq. 3. This subset of events contains less than 5% of the peak intensity, making this result of minor relevance for performing the Doppler-shift correction of the whole data set.

From this investigation, the conclusion can be drawn that, for the purpose of Doppler-shift correction, the spatial coordinates of the main interaction is at present a better choice than the first interaction found by a simple tracking algorithm based on the energy-angle relationship of the Compton effect. In terms of an experimental evaluation of the tracking concept, one needs to appreciate that its primary goal is to discriminate full-energy-peak γ-ray events in order to improve the peak-to-total ratio. This is not necessarily equivalent to finding the best approximation of the first interaction. But the tracking result is usable as

a quality benchmark, as shown by the improved peak shape when events with the first tracked interaction equal to the main interaction are considered.

4.3. In-beam γ-ray detection efficiency of GRETINA

The in-beam γ-ray detection efficiency of GRETINA was experimentally verified by analyzing the γ-ray yields of the various reaction products produced by multi-nucleon removal reactions from ^{36}Ar on a Be target at a beam energy of 85 MeV/u. The S800 spectrograph was set on the two-neutron removal channel leading to ^{34}Ar, but a wide variety of reaction products were collected in the spectrograph's focal plane. The very same measurement with the same spectrograph setting using the same 100 mg/cm^2 Be target had been performed in the past, using the well-characterized SeGA array [9], allowing the consistency of the yields extracted with both devices to serve as a benchmark here. The yields were extracted from the ratio of the efficiency-corrected full-energy peak counts from the Doppler-reconstructed γ-ray spectra and the number of reaction residues of the selected isotope collected at the S800 focal plane. The equality of the spectrograph acceptance in both experiments ensured the same population of excited states of the investigated nuclei. In figure 6, the γ-ray peak of the $2^+ \rightarrow 0^+$ transitions at 2091 keV in ^{34}Ar is shown, measured in GRETINA as well as with SeGA. For GRETINA, the singles spectrum Doppler-shift corrected with respect to the main interaction is considered, no add-back nor processing with a γ-ray tracking algorithm was applied.

In order to extract the counts in the full-energy peak from the spectrum, a fit based on GEANT simulations [16, 24] was performed and used to describe the background in the peak region, but not the peak itself. As seen in the previous section, the experimental Doppler-reconstructed peaks show significant tails to both sides and the resulting peak shape and hence the peak area is not well reproduced by the simulation. To describe the spectrum, the fit scales the simulated response spectra for the γ transitions dominating the region of several hundred keV width around the peak of interest and a single or double exponential function for describing the beam-induced background. For the peak

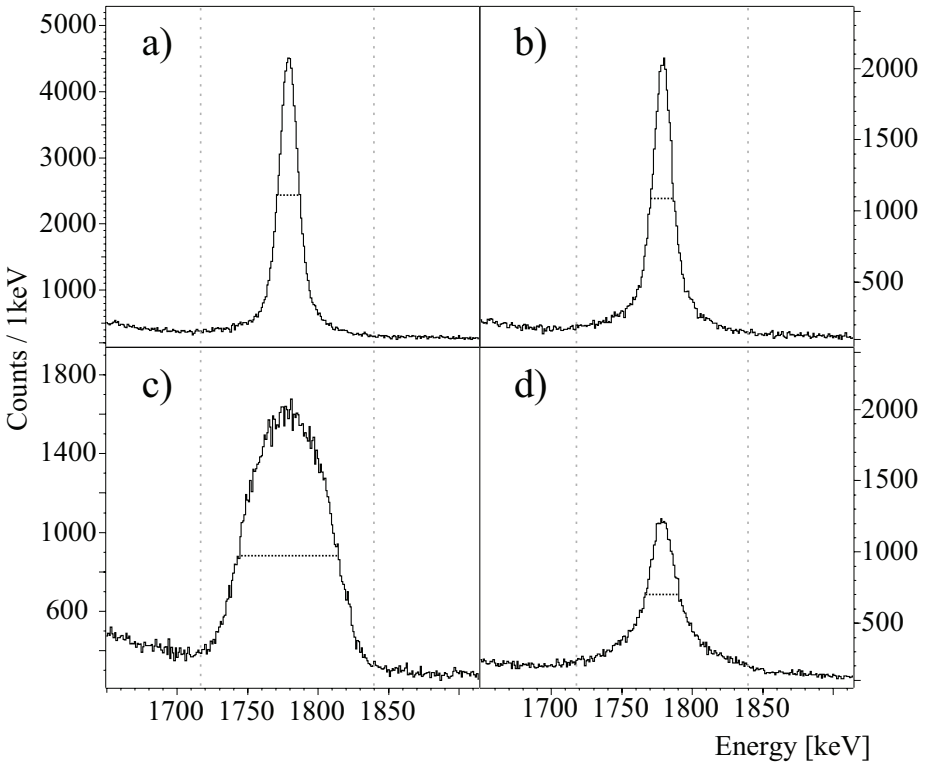

Figure 5: In-beam spectra of the 1779 keV transition using different approaches for the Doppler-shift correction are shown. The FWHM taken from the spectra are indicated as dashed lines. In a), the spatial coordinates of the main interaction are used, while in c) the coordinate of the segment center with the highest energy deposition is chosen for the Doppler reconstruction. For events where the first interaction obtained from a tracking algorithm is not identical with the main interaction, panel b) shows the peak using the main interaction point for Doppler reconstruction, while in panel d) the tracked first interaction point is used.

of interest, the simulated response spectrum is split into the contribution of events completely absorbed in the crystal (peak in spectrum) and γ-ray events scattered out of the crystal (Compton distribution in the spectrum). For the fitting, the latter spectrum is included and the spectrum region with the peak of interest is excluded in the fit. This approach allows to model the background underneath the peak as shown in figure 6 and peak counts can be extracted as the difference of simple integrals without assumptions about the peak shape. This also allows for a transparent error estimate, as the integral obtained from the measured spectrum follows the Poisson statistics. For simplicity, the same assumption can be applied to the integral obtained from the fit spectrum for estimating the background uncertainty. For both spectra shown in figure 6, this procedure results in a value for the peak integral with an uncertainty of 3%.

The in-beam efficiency for both devices was computed from the experimental source efficiency curve folded with the impact of the solid-angle relationship given by the Lorentz transformation and the effect of the Doppler shift which samples the efficiency curve at different γ-ray energies. The γ-yields for energies covering 800 keV to 3 MeV from the reaction residues ^{24}Mg, ^{26}Al, ^{28}Si, and ^{34}Ar were analyzed. The results show that beyond 1300 keV, the yields measured in SeGA and GRETINA agree within 4% and are well inside the uncertainties determined by the peak-count estimate from the spectra and the error made in the computation of the in-beam efficiency. For the lower energies, GRETINA results in 5-10% higher γ-ray yields compared to those measured in SeGA. Most likely, the background in the SeGA spectra for those cases was overestimated as the analyzed peaks reside on a significantly higher background than for the other cases. Furthermore, this energy region in the spectrum is contaminated with contributions from stopped γ-ray lines from beam-correlated background like the neutron edges in Ge or excitations of Al from the beam chamber induced by light particles from target breakup, for example. In GRETINA, those structures are smoothed out more in the Doppler-reconstruction process because of the higher granularity and the wider angle coverage, while in the reconstructed SeGA spectra, these background contributions result in local structures because

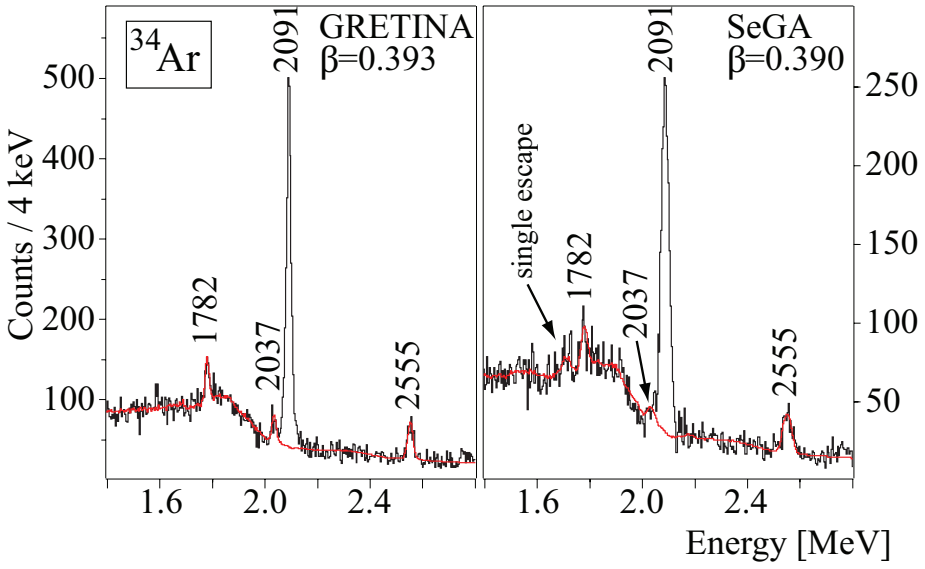

Figure 6: The Doppler-reconstructed spectra of the 2091 keV transition in ^{34}Ar measured in GRETINA and SeGA are shown, as well as a fit of the background underneath the peak area. The fit allows to determine the counts in the peak as simple integrals without any assumption about the shape of the peak itself.

of the more coarse, segment-based γ-ray detection angles. For the energies above 1300 keV the background is much lower as shown in the example in figure 6 and well described by the fit.

In conclusion, the experimental γ-ray yields measured with GRETINA and SeGA are consistent, verifying the absolute in-beam efficiency of GRETINA. It should be noted that this test not only confirms the correct functioning of the data acquisition system in the sense that no events were seem to be lost, but also suggests the correct processing of events in the decomposition computation. Losses due to wrong processing there would lead to events with erroneous spatial coordinates, hardly detectable with source measurements. For in-beam data, the correct spatial coordinates are crucial for a correct Doppler-shift reconstruction and any erroneous coordinates would have been detected as lower γ-ray yields obtained from the GRETINA data.

4.4. Analysis of γ-γ coincidences

The γ-γ coincidence spectrum quality achieved with in-beam data at intermediate beam energies is illustrated in figure 7. This figure shows the γ rays in coincidence with the 3991 keV $6^+ \rightarrow 4^+$ transition in ^{24}Mg from the same data set discussed in section 4.3. The spectra shown were analyzed with and without using the nearest-neighbor add-back procedure introduced in section 3.3. In the case of added-back events, the Doppler reconstruction is performed by selecting the first interaction point to be the *main* interaction from the crystal detecting the higher energy. The improvement utilizing the add-back procedure is evident in the spectra gated on the 3991 keV transition as well as in the projections from the γ-γ matrices (shown in the insets of figure 7). The $2^+ \rightarrow 0^+$ transition at 1369 keV is difficult to spot in the spectrum when treating GRETINA as individual crystals, but clearly identified when using the add-back approach. The transitions shown in the projection spectra have a significantly better peak-to-background ratio for the add-back, while in the other approach artifacts likely from cross scattering are evident. Those artifacts can easily be misinterpreted as peaks, e.g. the peak-like structure at about 4360 keV, which is clearly not seen in the projection of the add-back data. Also in the singles spectra (not shown), with or without add-back, no transition at this energy is apparent, while peaks at the other four energies are visible with consistent statistics.

This example demonstrates that the simple nearest-neighbor add-back procedure is an efficient approach for the analysis of γ-γ coincidence data obtained from fast-beam experiments. The quality of the spectra gated on a γ-ray transition is not significantly degraded by the remaining Compton scattering events, but by beam-correlated background and insufficient statistics. As shown in [20], dedicated tracking algorithms can reduce the amount of the remaining Compton scatters in the spectrum further, but at the expense of the full-energy-peak efficiency. Tracking cannot discriminate the beam correlated background further, as those events are emitted at random energies from the vicinity of the target. As shown in section 3.3, the nearest-neighbor add-back algorithm retains more than 90% of the calorimeter efficiency and is therefore a prudent choice for the

coincidence analysis of modest-statistics measurements with fast beams of rare isotopes.

Spectra employing the add-back procedure can be considered for extracting absolute γ-ray yields in a similar way as described for the singles spectra in section 4.3. But then the problem arises in the determination of the absolute efficiency. Add-back factors can only be determined reliably from γ-ray multiplicity 1 spectra, as seen in table 1 and discussed in section 3.3. This limits the data base for obtaining the efficiency curve for add-back spectra. Furthermore the impact of the same summing effect needs to be investigated for the in-beam spectra, especially for transitions from excited levels which have more than one decay branch. Lastly, the add-back factors, even at energies above 1 MeV, are quite sensitive to the energy thresholds as an appreciable fraction of add-back events stems from low-energy deposition in one of the detectors. Those considerations add into the uncertainties for the absolute efficiency and make it difficult to use add-back spectra for the determination of absolute γ-ray yields.

5. Summary

The performance of GRETINA has been an excellent match for the needs of the two in-beam γ-ray spectroscopy campaigns at NSCL using intermediate-energy beams. While GRETINA is ultimately a γ-ray tracking array, data obtained in typical experiments with fast beams of rare isotopes can be analyzed efficiently without employing sophisticated tracking algorithms for reconstructing the Compton scattering sequences of γ-ray events. It was shown that for successful Doppler reconstruction, the selection of the *main* (highest-energy) interaction from the reported interaction points is a viable approach. The quality of the Doppler-shift corrected singles spectra is usually sufficient for determining the peak counts and for these spectra, an absolute in-beam efficiency can be computed accurately from an experimental efficiency curve based on source measurements in a transparent way to extract the absolute γ-ray yields. For the analysis of γ-γ coincidences, a simple nearest-neighbor add-back approach was

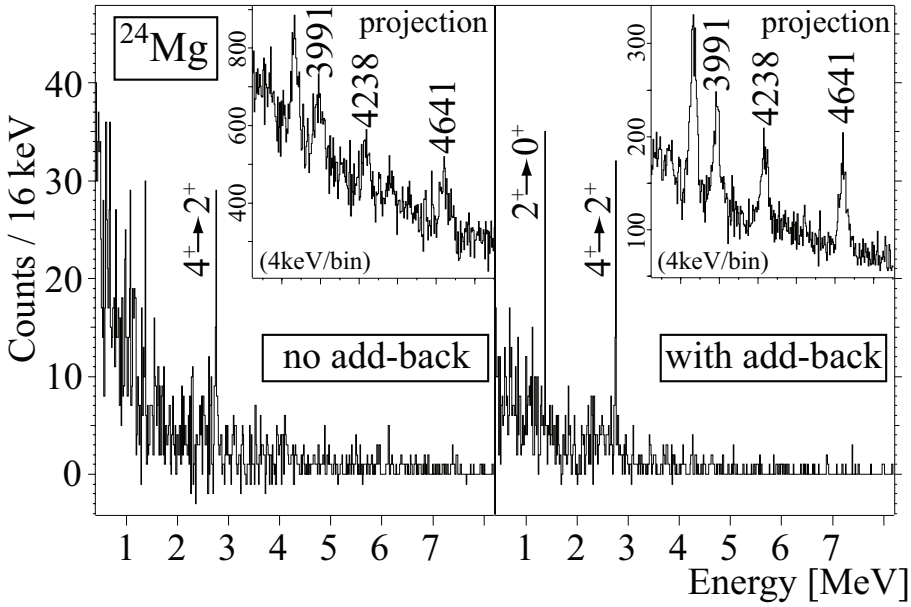

Figure 7: The Doppler-corrected coincidence spectra cut on the $6^+ \rightarrow 4^+$ transition at 3991 keV in ^{24}Mg are shown. A background spectrum was obtained from a cut covering the region from 4.4 to 4.6 MeV and subtracted. On the right, the add-back procedure is used; on the left, GRETINA is treated as individual crystals. The insets show the projections of the γ-γ coincidence matrices in which the cuts were made. The improvement of the spectral quality using the simple add-back algorithm is evident.

introduced as an efficient tool that delivers good spectral quality in terms of the peak-to-total ratio while retaining more than 90% of the maximum achievable calorimeter efficiency. This simple treatment of the γ-ray data in the analysis is justified by the low γ-ray multiplicities at which they are produced in experiments with fast beams of rare isotopes.

6. Acknowledgement

This work was supported by the NSF under Grant No. PHY-1102511. GRETINA was funded by the DOE, Office of Science. Operation of the array at NSCL was supported by the NSF under Cooperative Agreement No. PHY-1102511 (first NSCL campaign), the DOE under Grant No. DE-AC02-05CH11231 (LBNL) and Grant No. DE-SC0014537 (second NSCL campaign).

References

[1] A. Gade and T. Glasmacher, Prog. in Part. and Nucl. Phys. 60 (2008) 161.

[2] T. Glasmacher, Annu. Rev. Nucl. Part. Sci. 48 (1998) 131.

[3] A. Gade, Eur. Phys. J. A 51 (2015) 118.

[4] S. Takeuchia, T. Motobayashia, Y. Toganob, M. Matsushitac, N. Aoid, K. Demichie, H. Hasegawae, H. Murakamia, Nuclear Instruments and Methods in Physics Research Section A: Accelerators, Spectrometers, Detectors and Associated Equipment 763 (2014) 596.

[5] D. Weisshaar, A. Gade, T. Glasmacher, G. F. Grinyer, D. Bazin, P. Adrich, T. Baugher, J. M. Cook C. Aa. Diget, S. McDaniel, A. Ratkiewicz, K. P. Siwek, K.A. Walsh, Nuclear Instruments and Methods in Physics Research Section A: Accelerators, Spectrometers, Detectors and Associated Equipment 624 (2010) 615.

[6] S. Shimoura, Nuclear Instruments and Methods in Physics Research Section A: Accelerators, Spectrometers, Detectors and Associated Equipment 525 (2004) 188.

[7] H. J. Wollersheim, D. E. Appelbe, A. Banu, R. Bassini, T. Beck, F. Becker, P. Bednarczyk, K.-H. Behr, M. A. Bentley, G. Benzoni, C. Boiano, U. Bonnes, A. Bracco, S. Brambilla, A. Brünle, A. Bürger, K. Burkard, P. A. Butler, F. Camera, D. Curien, J. Devin, P. Doornenbal, C. Fahlander, K. Fayz, H. Geissel, J. Gerl, M. Górska, H. Grawe, J. Grebosz, R. Griffiths, G. Hammond, M. Hellström, J. Hoffmann, H. Hübel, J. Jolie, J.V. Kalben, M. Kmiecik, I. Kojouharov, R. Kulessa, N. Kurz, I. Lazarus, J. Li J. Leske, R. Lozeva, A. Maj, S. Mandal, W. Meczyński, B. Million, G. Münzenberg, S. Muralithar, M. Mutterer, P.J. Nolan, G. Neyens, J. Nyberg, W. Prokopowicz, V. F. E. Pucknell, P. Reiter, D. Rudolph, N. Saito, T. R. Saito, D. Seddon, H. Schaffner, J. Simpson, K.-H. Speidel, J. Styczeń, K. Sümmerer, N. Warr, H. Weick, C. Wheldon, O. Wieland, M. Winkler, M. Ziebliński, Nuclear Instruments and Methods in Physics Research Section A: Accelerators, Spectrometers, Detectors and Associated Equipment 537 (2005) 637.

[8] J. Eberth, G. Pascovici, H. G. Thomas, N. Warr, D. Weisshaar, D. Habs, P. Reiter, P. Thirolf, D. Schwalm, C. Gund, H. Scheit, M. Lauer, P. Van Duppen, S. Franchoo, M. Huyse, R. M. Lieder, W. Gast, J. Gerl, K. P. Lieb, Prog. Part. Nucl. Phys. 46 (2001) 389.

[9] W. F. Mueller, J .A. Church, T. Glasmacher, D. Gutknecht, G. Hackman, P. G. Hansen, Z. Hu, K. L. Miller, and P. Quirin, Nuclear Instruments and Methods in Physics Research Section A: Accelerators, Spectrometers, Detectors and Associated Equipment 466 (2001) 492.

[10] D. Bazin, J. A. Caggiano, B. M. Sherrill, J. Yurkon, A. Zeller, Nuclear Instruments and Methods in Physics Research Section B: Beam Interactions with Materials and Atoms 204 (2003) 629

[11] A. Gade, B. M. Sherrill, Physica Scripta 91, 053003 (2016)

[12] S. Paschalis, I. Y. Lee, A. O. Macchiavelli, C. M. Campbell, M. Cromaz, S. Gros, J. Pavan, J. Qian, R. M. Clark, H. L. Crawford, D. Doering, P. Fallon, C. Lionberger, T. Loew, M. Petri, T. Stezelberger, S. Zimmermann, D. C. Radford, K. Lagergren, D. Weisshaar, R. Winkler, T. Glasmacher, J. T. Anderson, C. W. Beausang, Nuclear Instruments and Methods in Physics Research Section A: Accelerators, Spectrometers, Detectors and Associated Equipment 709 (2013) 44

[13] M. A. Deleplanque, I. Y. Lee, K. Vetter, G. J. Schmid, F. S. Stephens, R. M. Clark, R. M. Diamond, P. Fallon, A. O. Macchiavelli, Nuclear Instruments and Methods in Physics Research Section A: Accelerators, Spectrometers, Detectors and Associated Equipment 430 (1999) 292

[14] P. Fallon, A. Gade, and I-Y. Lee, Annu. Rev. of Nucl. and Part. Sci. 66 (2016) in press. doi 10.1146/annurev-nucl-102115-044834

[15] H. Iwasaki, A. Dewald, T. Braunroth, C. Fransen, D. Smalley, A. Lemasson, C. Morse, K. Whitmore, C. Loelius, Nuclear Instruments and Methods in Physics Research Section A: Accelerators, Spectrometers, Detectors and Associated Equipment 806 (2016) 123

[16] L. A. Riley, M. L. Agiorgousis, T. R. Baugher, D. Bazin, M. Bowry, P. D. Cottle, F. G. DeVone, A. Gade, M. T. Glowacki, K. W. Kemper, E. Lunderberg, D. M. McPherson, S. Noji, F. Recchia, B. V. Sadler, M. Scott, D. Weisshaar, R. G. T. Zegers, Phys. Rev. C 90, 011305(R) (2014)

[17] M. Cromaz, V. J. Riot, P. Fallon, S. Gros, I. Y. Lee, A. O. Macchiavelli, C. Vu, H. Yaver, S. Zimmermann, Nuclear Instruments and Methods in Physics Research Section A: Accelerators, Spectrometers, Detectors and Associated Equipment 597 (2008) 233

[18] J. T. Anderson, R. Brito, D. Doering, T. Hayden, B. Holmes, J. Joseph, H. Yaver, S. Zimmermann, IEEE Transactions on Nuclear Science NS-56 (2009) 258

[19] S. Zimmermann, J. T. Anderson, D. Doering, J. Joseph, C. Lionberger, T. Stezelberger, H. Yaverm, IEEE Transactions on Nuclear Science 59 (2012) 2494

[20] T. Lauritsen, A. Korichi, S. Zhu, A. N. Wilson, D. Weisshaar, J. Dudouet, A. D. Ayangeakaa, M. P. Carpenter, C. M. Campbell, E. Clément, H. L. Crawford, M. Cromaz, P. Fallon, J. P. Greene, R. V. F. Janssens, T. L. Khoo, N. Lalovi, I. Y. Lee, A. O Macchiavelli, R. M. Perez-Vidal, S. Pietri, D. C. Radford, D. Ralet, L. A. Riley, D. Seweryniak, O. Stezowski, Nuclear Instruments and Methods in Physics Research Section A: Accelerators, Spectrometers, Detectors and Associated Equipment 836 (2016) 46

[21] International Atomic Energy Agency, IAEA TECDOC No. 619

[22] K. Siegbahn, Alpha, Beta and Gamma-ray Spectroscopy, North Holland (1965)

[23] A. Gade, J. A. Tostevin, V. Bader, T. Baugher, D. Bazin, J. S. Berryman, B. A. Brown, D. J. Hartley, E. Lunderberg, F. Recchia, S. R. Stroberg, Y. Utsuno, D. Weisshaar, K. Wimmer Phys. Rev. C 93, 031601(R) (2016)

[24] S. Agostinelli et al. (GEANT4 Collaboration), Nuclear Instruments and Methods in Physics Research Section A: Accelerators, Spectrometers, Detectors and Associated Equipment 506 (2003) 250